Geophysical Research Letters

RESEARCH LETTER
10.1029/2020GL087267

Contribution of Sea-State Dependent Bubbles to Air-Sea Carbon Dioxide Fluxes

B. G. Reichl[1,2] **and L. Deike**[3,4]

[1]Program in Atmospheric and Oceanic Science, Princeton University, Princeton, NJ, USA, [2]NOAA Geophysical Fluid Dynamics Laboratory, Princeton, NJ, USA, [3]Department of Mechanical and Aerospace Engineering, Princeton University, Princeton, NJ, USA, [4]Princeton Environmental Institute, Princeton University, Princeton, NJ, USA

Key Points:
- We estimate globally sea-state dependent carbon dioxide fluxes with a novel gas transfer parameterization
- Bubbles support approximately 40% of the carbon dioxide uptake by the ocean
- The bubble contribution and sea-state dependence is highly variable on regional and seasonal scales

Correspondence to:
B. G. Reichl,
brandon.reichl@noaa.gov

Citation:
Reichl, B.G, & Deike, L. (2020). Contribution of sea-state dependent bubbles to air-sea carbon dioxide fluxes. *Geophysical Research Letters*, *47*, e2020GL087267. https://doi.org/10.1029/2020GL087267

Received 27 JAN 2020
Accepted 17 MAR 2020
Accepted article online 22 MAR 2020

Abstract Breaking surface ocean waves produce bubbles that are important for air-sea gas exchanges, particularly during high winds. In this study we estimate air-sea CO_2 fluxes globally using a new approach that considers the surface wave contribution to gas fluxes. We estimate that 40% of the net air-sea CO_2 flux is via bubbles, with annual, seasonal, and regional variability. When compared to traditional gas-flux parameterization methods that consider the wind speed alone, we find high-frequency (daily to weekly) differences in the predicted gas flux using the sea-state dependent method at spatial scales related to atmospheric weather (10 to 100 km). Seasonal net differences in the air-sea CO_2 flux due to the sea-state dependence can exceed 20%, with the largest values associated with North Atlantic and North Pacific winter storms. These results confirm that bubbles are important for global gas-flux dynamics and that sea-state dependent parameterizations may improve performance of global coupled models.

1. Introduction

A paramount challenge at present is to understand how increased concentrations of carbon dioxide will be distributed between the atmospheric, terrestrial, and oceanic systems. Estimates are that 40% of anthropogenic carbon dioxide (CO_2) currently resides in the atmosphere, while 20–30% has passed to the ocean (Garbe et al., 2014; IPCC, 2014; Landschützer et al., 2014; Le Quére, 2018; Resplandy et al., 2018). These estimates derive from both observational (e.g., Rödenbeck et al., 2015) and modeling (e.g., Le Quére, 2018) approaches. The air-sea CO_2 flux is often estimated from parameters including the CO_2 concentration in the ocean (C_o, mol m^{-3}), the CO_2 partial pressure in the atmosphere (p_a, kg m^{-1} s^{-2}), the CO_2 solubility in seawater (K_0, mol s^2 kg^{-1} m^{-2}), and the transfer "piston" velocity (k_w, m s^{-1}) (Wanninkhof et al., 2009; Woolf, 1993):

$$F = k_w \left(C_o - K_0 \, p_a \right). \tag{1}$$

Woolf et al. (2019) conclude that the dominant remaining uncertainties in estimates of net global CO_2 fluxes are due to insufficient global sampling and knowledge on the air-sea transfer velocity. One source of uncertainty in determining air-sea transfer velocity comes from parameterizing the effects of bubbles produced by breaking waves. The bubbles introduce variability in CO_2 transfer velocities in high-latitudes that is only captured by considering the surface wave (sea-state) variability (Fangohr & Woolf, 2007).

The bubbles that contribute to the air-sea gas flux form as air entrained under breaking waves (Farmer et al., 1993; Keeling, 1993; Thorpe & Humphries, 1980; Woolf, 1997). These bubbles enhance gas exchange in many ways, including increasing air-sea contact area, enhancing near-surface turbulent mixing, and a hydrostatic pressure effect (submerged bubbles are squeezed by the weight of water above) (e.g., Garbe et al., 2014). The relative importance of these effects depends on the bubble size and the gas solubility in seawater. For example, the net air-sea gas flux of more soluble gases (e.g., CO_2) is less enhanced by pressure effects than less soluble gases (e.g., oxygen and argon) (Keeling, 1993; Woolf, 1993, 2005). The contribution of bubbles to global air-sea CO_2 flux was estimated by Woolf (1997) by assuming that bubble-mediated transfer velocity is proportional to the whitecap fraction: $k_{wB} \propto W$ (Keeling, 1993; Woolf, 1997). Their study suggests that bubbles contribute about 30% of the global CO_2 transfer velocity.

Deike and Melville (2018, hereafter DM18) developed a sea-state dependent gas transfer velocity parameterization. The DM18 parameterization is based on direct numerical simulation of bubble dynamics under

breaking waves (Deike et al., 2016) together with observations and modeling of the wave and wave breaking statistics (see Deike et al., 2017) and validated against field measurements of the gas transfer velocity (Bell et al., 2017; Brumer et al., 2017). In this study we utilize this novel sea-state dependent gas transfer velocity parameterization (see section 2) together with estimates of the global wind and wave fields at three-hourly time increments and ~50 km (0.5°) spatial resolution (see section 3) to investigate the role of bubbles in air-sea CO_2 flux and reveal how variability in the sea-state (due to storm waves, swell waves, etc.) contributes to variability in the flux. Through the application of these methods (sections 4 and 5) we find that accounting for sea-state when computing CO_2 flux changes its value by up to 20% with large-scale coherent spatial patterns that are likely of important consequence for global CO_2 flux modeling. These results demonstrate that considering the sea-state in CO_2 flux parameterizations has important implications for estimating air-sea CO_2 fluxes and for reducing uncertainties in quantifying CO_2 budgets.

2. Parameterizing the Air-Sea CO_2 Flux

In this section we review the wind only and sea-state dependent (DM18) approaches that are used to parameterize k_w in this study.

2.1. Wind-Only Approach

Traditional parameterizations for the gas transfer velocity, k_w, reflect correlation with wind speed, such as in Wanninkhof (2014, hereafter W14) and Ho et al. (2006):

$$k_w^{W14} = C_{W14} U_{10}^2 \left(\frac{Sc}{660}\right)^{-1/2}, \tag{2}$$

where Sc is the Schmidt number ($Sc = \nu/D$, which relates the fluid viscosity, ν [$m^2\ s^{-1}$], to the gas diffusivity, D [$m^2\ s^{-1}$]), U_{10} is 10-m wind speed (m s^{-1}), and $C_{W14} = 0.251$ (cm hr^{-1}) ($m^2\ s^{-2}$)$^{-1}$, yielding k_w in conventional units of cm hr^{-1}. The CO_2 transfer velocity is often given relative to $Sc = 660$, which is the value of Sc for CO_2 in seawater at 20°C ($k_w^{660} = k_w(Sc/660)^{1/2}$). The power dependence on U_{10} (here quadratic) is an empirical result obtained when considering mean wind speed dependence in laboratory and field studies. The transfer velocity coefficient (here C_{W14}) is often constrained using bulk field observations, such as global bomb C14 observations and tracer budget experiments (see the review by Wanninkhof et al., 2009). When the coefficient and power are calibrated using in situ data, the transfer velocity contains the average bubble contribution to gas transfer present during the observation periods. Calibration of the coefficient is common for different wind product applications due to both uncertainty in the large-scale constraints and differences in time-averaging of the mean U_{10}.

2.2. Sea-State Dependent Approach

In Deike and Melville (2018), the effects of sea-state on k_w are included by expressing the gas transfer velocity as the sum of non-bubble k_{wNB} and bubble k_{wB} components (following Keeling, 1993; Woolf, 1997, 2005):

$$k_w^{DM18} = k_{wNB} + k_{wB}. \tag{3}$$

The bubble-mediated gas transfer velocity k_{wB} in (3) is found by DM18 to vary with significant wave height, H_s (m), and wind friction, u_* (m s^{-1}):

$$k_{wB} = \frac{A_B}{K_0\ R\ T_0} u_*^{5/3} (g\ H_s)^{2/3} \left(\frac{Sc}{660}\right)^{-1/2}, \tag{4}$$

where A_B is a dimensional fitting coefficient (DM18 find $A_B = 1 \pm 0.2 \times 10^{-5}\ s^2\ m^{-2}$), R is the ideal gas constant, T_0 is the sea surface temperature (here skin temperature measured from satellites), and g is gravitational acceleration. Wave breaking tendency (responsible for bubble formation) depends on the high-frequency tail of the wave spectrum and can be formulated with additional characteristics of the wave field, such as the period of the most energetic waves (T_p). While DM18 considered such parameters in determining k_{wB}, the leading order sea-state dependent effects were captured from H_s alone in their data (related to an inherent relationship of T_p to H_s and u_*). The non-bubble gas transfer velocity k_{wNB} in DM18 is found from

$$k_{wNB} = A_{NB} u_* \left(\frac{Sc}{660}\right)^{-1/2}, \tag{5}$$

where A_{NB} is an empirical, nondimensional coefficient given as 1.55 $\times 10^{-4}$, corresponding to the the COAREG coefficient $A = 1.5$ (Fairall et al., 2011). Variations of about 30% for this coefficient can be found in the literature (Bell et al., 2017; Blomquist et al., 2017; Fairall et al., 2011; Smith et al., 2018; Yang et al., 2014).

In this study we apply the DM18 approach to investigate sea-state dependence of air-sea CO_2 flux, but other approaches to consider wave breaking and sea-state dependence exist (Brumer et al., 2017; Woolf, 2005; Zhang, 2012; Zhao et al., 2003). For example, Brumer et al. (2017) find similar mean parameter dependency in k_w but expressed using wave Reynolds number ($Re_H = \frac{u_* H_s}{\nu}$). The wave Reynolds number approach is constrained dimensionally to give equal weight to u_* and H_s, while the larger exponent for u_* than H_s in k_{wB} of DM18 arises from scaling of the breaking probability distribution function. While this could indicate enhanced sea-state induced variability in wave Reynolds number based parameterizations, we note that DM18 found generally consistent results for CO_2 between the two approaches. More complex approaches to parameterize bubble-mediated air-sea gas flux for less soluble gases like oxygen and nitrogen also separate the potential terms in parenthesis of equation (1) into bubble and non-bubble components (e.g., Leighton et al., 2018; Zhang, 2012; Liang et al., 2013). Such approaches reduce dependence on seawater solubility and permit super-saturated gas concentration in the ocean. This super-saturation effect is less important for more soluble gases, including carbon dioxide (Liang et al., 2013; Woolf, 1993) and therefore is not investigated here.

3. Data Description

The bulk formula for air-sea carbon dioxide flux (1) can also be written:

$$F_{CO_2} = k_w \left(K_0 \, \Delta p_{CO_2} \right), \tag{6}$$

where the carbon dioxide concentration difference is expressed as the product of solubility K_0 and air-sea partial pressure difference (Δp_{CO_2}) (see Wanninkhof et al., 2009). To investigate global fields of k_w and air-sea CO_2 flux we combine several observational and model derived data sets needed to apply equations (3), (4), (5), and (6). We obtain global fields needed to model wind friction (u_*), wave height (H_s), solubility (K_0), and carbon concentration difference ($\Delta \, p_{CO_2}$) spanning from 1982 to 2015. These fields are described in this section.

3.1. Wind Product

Atmospheric wind velocity is used to estimate wind friction (u_*) and as an input to simulate the wave height (section 3.2). We employ the Japanese Meteorological Society Reanalysis product (JRA55-do), which includes 50 years of 10-m wind vectors (U_{10}) at approximately half-degree resolution every 3 hr (Kobayashi et al., 2015; Tsujino et al., 2018). JRA55-do uses hindcasting, data assimilation, and various statistical constraints to produce a realistic atmospheric state estimate (see Taboada et al., 2019) and was selected by the World Climate Research Program's sixth Coupled Model Intercomparison Project for forcing ocean-ice model experiments (CMIP6, see Griffies et al., 2016). We conducted similar experiments from the CORE atmospheric reanalysis (Large & Yeager, 2009) and found qualitatively similar results.

The wind friction velocity u_* is estimated from U_{10} using a bulk formula parameterization (Edson et al., 2013). The atmospheric stability is also important in determining u_* if there is a sufficiently strong buoyancy gradient. However, it is primarily high wind events that contribute to k_{wB}, a regime where the atmospheric stability effect is typically small; therefore, we neglect the stability effect here.

3.2. Wave Height

Global wave fields are simulated for this study with WAVEWATCH-III (hereafter WW3, The WAVEWATCH III Development Group (WW3DG), 2016). WW3 is a third-generation surface wave model developed at the National Oceanographic and Atmospheric Administration's National Center for Environmental Prediction (NCEP) and Environmental Modeling Center. To simulate the waves there are choices of wave model physics parameterizations within WW3. We employ NCEP default physics options from model release v5.16. These defaults include the ST4 forcing package based on Ardhuin et al. (2010) and have been previously verified using NCEP's Climate Forecast System Reanalysis (Chawla et al., 2013). Modern wave model physics parameterizations are often optimized using observed wave height from buoy and satellite observations and therefore provide similar results for wave height in typical conditions. However, spectral properties such as peak period can be more sensitive to choices in such parameterizations, especially under high wind

conditions (e.g., Liu et al., 2017). Furthermore, observational challenges dictate that model performance over large swaths of the ocean remains under-analyzed, though methods to observe high wind and remote locations are emerging (e.g., Thomson et al., 2018).

For this simulation the WW3 spectral resolution is 25 frequencies by 24 directions with spatial resolution equivalent to the JRA55-do forcing grid (half-degree) to fully exploit the relatively high reanalysis resolution. Inputs to the wave model include JRA55-do wind vectors and monthly varying sea-ice from a coupled ocean sea-ice simulation forced with the JRA55-do fields (see Adcroft et al., 2019). Ocean currents induce additional sea-state heterogeneity due to wave refraction and other wave-current interactions but are not included in this study. The wave height statistics from the JRA55-do simulation agree well with Chawla et al. (2013) when considering small differences in the wind (not shown). Since a focus of this study is to reduce uncertainty in gas transfer velocity estimation due to sea-state, we provide the significant wave height from these simulations at doi.org/10.5281/zenodo.3626120.

3.3. Seawater Solubility

The solubility K_0 is estimated from the sea surface temperature (T_0) and surface salinity (S_0) with the empirical relationship of (Weiss, 1974):

$$\ln(K_0) = a_1 + a_2\frac{100}{T_0} + a_3 * \ln\left(\frac{T_0}{100}\right) + S_0\left(b_1 + b_2\frac{T_0}{100} + b_3\left(\frac{T_0}{100}\right)^2\right), \quad (7)$$

where T_0 is in absolute temperature (Kelvin) and S_0 is in g kg^{-1} (coefficients are $a_1 = -60.2409$, $a_2 = 93.4517$, $a_3 = 23.3585$, $b_1 = 0.023517$, $b_2 = -0.023656$, and $b_3 = 0.0047036$ for K_0 in units of moles (kg·atm)$^{-1}$). Monthly mean T_0 comes from NOAA/NCEP's Optimum Interpolation (OI) SST V2 (https://www.emc.ncep.noaa.gov/research/cmb/sst_analysis/), which is available from 1982 onward at one-degree resolution. Similar time series of surface salinity do not exist, so we employ a monthly mean salinity climatology (Zweng et al., 2013).

3.4. Carbon Dioxide Partial Pressure (Δp_{CO_2}) Climatology

The air-sea partial pressure difference of carbon dioxide is not observed globally, but many discrete time series exist (see Rödenbeck et al., 2015, for discussion on various products and interpolation methods). The available oceanic pCO_2 data are synthesized in the Surface Ocean CO_2 Atlas (SOCAT) database (Pfeil et al., 2012; Sabine et al., 2012). Landschützer et al. (2014) used a neural-network method to construct global estimates of this quantity at one-degree resolution. Their method is used here to provide monthly Δp_{CO_2} spanning from 1982 to 2015 (https://www.nodc.noaa.gov/ocads/oceans/SPCO_2_1982_2015_ETH_SOM_FFN.html).

3.5. Global Field Analysis

Snapshots via punctual model outputs and climatology computed from this study are given in Figure 1. The snapshot fields demonstrate significant spatial and temporal variability associated with atmospheric weather events (50–100 km of horizontal scale) that dominates instantaneous wind, wave, and transfer velocity patterns (Figures 1a–1c). The mean climatology of these fields demonstrates how these events correspond to mean global wind patterns that are reflected in the wave and transfer coefficient fields (Figures 1d–1f). General correlation between wind, wave, and gas transfer patterns is seen, particularly in climatological averages. The wind and wave field patterns are least correlated in the presence of high wind storm events (where sea-state varies along the storm path) and nonlocal swells (where wave heights are not driven locally). These events indicate where the sea-state dependence of the gas transfer velocity k_w is expected to be most important for determining the CO_2 flux. These differences are largest in the punctual fields, but key large-scale differences exist in the climatology due to fetch effects associated with prevailing wind direction and land configuration. For example, the eastern North Atlantic and North Pacific show enhanced wave heights associated with the dominant westerly winds.

The bubble contribution to the gas transfer velocity is proportional to $k_{wB} \propto u_*^{5/3} g {H_s}^{2/3}$ while the non-bubble contribution is proportional to $k_{wNB} \propto u_*$. The bubble contribution to total gas transfer is thus stronger in high wind and wave conditions, physically linked to increasing wave energy and air entrainment. The DM18 bubble contribution to gas transfer velocity, k_{wB}, exceeds the non-bubble contribution, k_{wNB}, for wind speeds greater than 17 m s^{-1} (see DM18 and section 4). The percentage of time where the wind exceeds 17 m s^{-1} therefore indicates where bubble-mediated gas transfer is the dominant component of the transfer velocity.

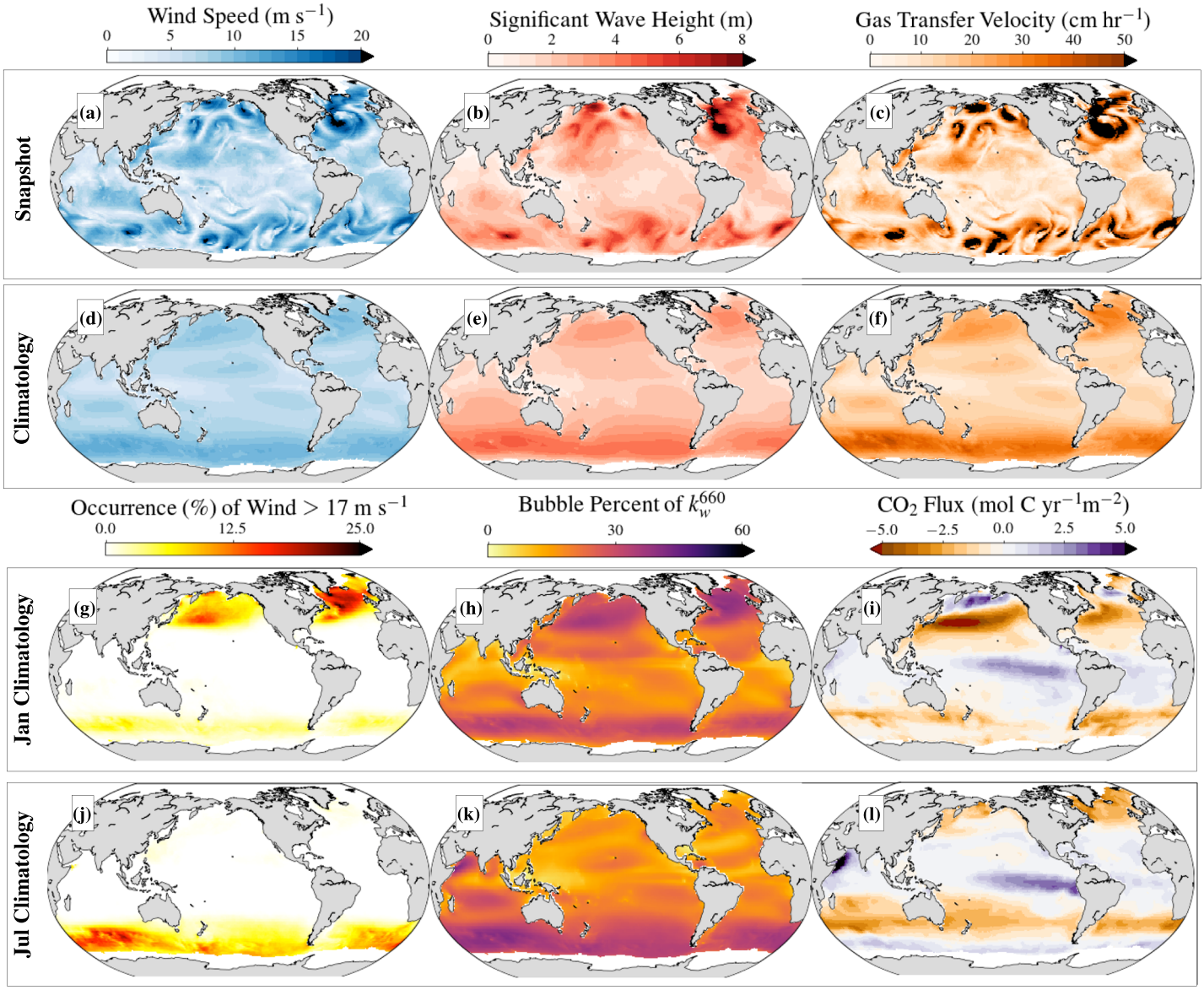

Figure 1. Snapshot and climatological mean of (a, d) 10-m wind speed (U_{10}), (b, e) significant wave height (Hs), and (c, f) k_w^{660} total gas transfer velocity (from the sea-state formulation, equation (3)). January (g–i) and July (j–l) climatological mean for the $U_{10} > 17$ m s^{-1} occurrence (g, j), used as a proxy for where bubbles account for 50% of total gas transfer velocity; the ratio of bubble contribution to total gas transfer velocity k_{wB}^{660}/k_w^{660} (h, k), and the net air-sea CO_2 flux (from equation 6) (i, l).

The January and July mean of this threshold occurrence exhibit strong seasonality, with values exceeding 20% in high-latitude winters (Figures 1g and 1j). These regions play a significant role in atmosphere-ocean carbon dioxide exchange, suggesting important bubble induced contributions (e.g.,Landschützer et al., 2014; Takahashi et al., 1997). From equation (3), we diagnose the fraction of the gas transfer velocity due to bubbles (k_{wB}/k_w, Figures 1h and 1k), indicating similar regional and seasonal patterns to those observed on the 17 m s^{-1} wind speed threshold occurrence.

However, the January and July mean climatology of the net air-sea CO_2 flux (Figures 1i and 1l) suggest that the sea-state dependence of the gas transfer velocity alone cannot completely describe the sea-state effects on CO_2 flux patterns. The sign and magnitude of the carbon concentration differences (Δp_{CO_2}) are not correlated to the wave patterns, which suggests that certain regions with high wind and wave activity will contribute more to global net CO_2 fluxes (see further discussion in section 5.2). Thus, the wave contributions to the transfer velocity and the wave contributions to the net CO_2 flux must be considered together.

4. Global Constraints and Flux

The coefficient in the sea-state formulation (A_B in (4)) is determined using field data where the gas transfer velocity is computed from fluxes via eddy covariance methods (Bell et al., 2017; Brumer et al., 2017). The eddy covariance flux methods yield higher transfer velocity at a given wind speed than methods calibrated to bomb C14 or tracer measurements that integrate the flux over longer periods (12 hr to several days) and larger spatial areas, though the reasons for the differences remain poorly understood (Ho et al., 2006, 2011; Wanninkhof et al., 2009; Wanninkhof, 2014). Furthermore, in DM18, all observed data (including wind and wave observations) are averaged into relatively high-frequency bins (20–30 min) compared to the temporal variance captured by the atmospheric forcing (3 hr) used in this study. In order to focus on sea-state added variability, we calibrate the bubble coefficient A_B to yield global mean k_w values in agreement with the one from Wanninkhof (2014), used in recent global carbon budget estimates (e.g., Landschützer et al., 2014; Le Quére, 2018; Rödenbeck et al., 2015).

4.1. Calibrating the Sea-State Formulation Using Global k_w Constraints

The average wind speed dependence of the gas transfer velocity from the original sea-state formulation (DM18) is shown in Figure 2a (diamonds) and exceeds the wind-only parameterization (W14) at all wind speeds (thick red line). As discussed in Wanninkhof et al. (2009), even for wind-only gas transfer velocity, the coefficient in equation (2) is routinely adjusted for the wind product to obtain consistent global mean gas transfer velocity. A canonical value for the global mean $\langle k_w^{660} \rangle \approx 16$ cm hr^{-1} (see Ho et al., 2006; Landschützer et al., 2014; Wanninkhof et al., 2009; Wanninkhof, 2014) is often used, but the coefficient remains highly uncertain (Woolf et al., 2019). The DM18 climatological global mean without calibration is $\langle k_{wDM18,original}^{660} \rangle = 19.19$ cm hr^{-1}, which is significantly higher than both the canonical value and the global mean using the wind-only W14 formulation in our study $\langle k_{wW14}^{660} \rangle = 14.90$ cm hr^{-1} (see Figure 2b, red line). We therefore calibrate the sea-state dependent DM18 formulation (coefficients in equation (4)) such that the global mean gas transfer velocity $\langle k_{wDM18}^{660} \rangle$ is consistent with this W14 value. This is done by multiplying a factor of 77.5% times both the bubble and non-bubble components of the gas transfer velocity (Figure 2a, squares) leading to $\langle k_{wDM18}^{660} \rangle = 14.88$ cm hr^{-1} (Figure 2b, black line). Results presented hereafter include this 77.5% calibration factor. Note that a similar mean global gas transfer velocity could be obtained by making different calibration choices.

4.2. Globally Integrated Transfer Velocity and Net CO_2 Fluxes

The calibration described in the previous section dictates that similar global mean gas transfer velocity is found between the sea-state (DM18) and wind-only (W14) formulations by construction (solid lines in Figure 2b). Figure 2c shows the net globally integrated carbon dioxide flux F_{CO_2} estimated in this study from 1982 to 2015 is also made similar by the calibration. The average value of the net CO_2 flux over the whole period using the calibrated sea-state method is -1.24 ± 0.48 pg C year^{-1}, in the range of previous studies (e.g., Landschützer et al., 2014).

The average contribution by bubbles to the net CO_2 flux is diagnosed from the sea-state dependent approach as -0.50 ± 0.16 pg C year^{-1}. The bubble contribution to the gas transfer velocity (k_{wB}/k_w) is roughly 30% over the entire time series (Figure 2d, dashed line), in agreement with the estimate of Woolf (1997). The contribution of bubbles to global CO_2 flux from F_{CO_2}, however, is on average about 40%, with significant monthly to yearly variability (solid line). The relative contribution of bubbles to the CO_2 flux is higher than their contribution to the gas transfer velocity largely because of the sign bias in the flux. This bias arises because in the equatorial regions, CO_2 is degassed to the atmosphere with little bubble contribution. Therefore, when considering the net flux, the net contribution of the degassing region is to increase the percentage of bubble contribution. The interannual variability in the CO_2 flux is not seen in the gas transfer velocity and therefore must instead be primarily related to long-term trends and internal variability in $\Delta\, p_{CO_2}$ (Rödenbeck et al., 2015).

5. Influence of Sea-State Dependence on Parameterized Air-Sea CO_2 Flux

The different spatial patterns of the wind and wave fields (see Figure 1) result in differences in the gas transfer velocity when comparing the sea-state dependent and wind-only parameterizations. We now investigate in detail the differences between the gas transfer velocity predicted by the sea-state dependent formulation and the wind-only formulation and the implications for air-sea CO_2 flux.

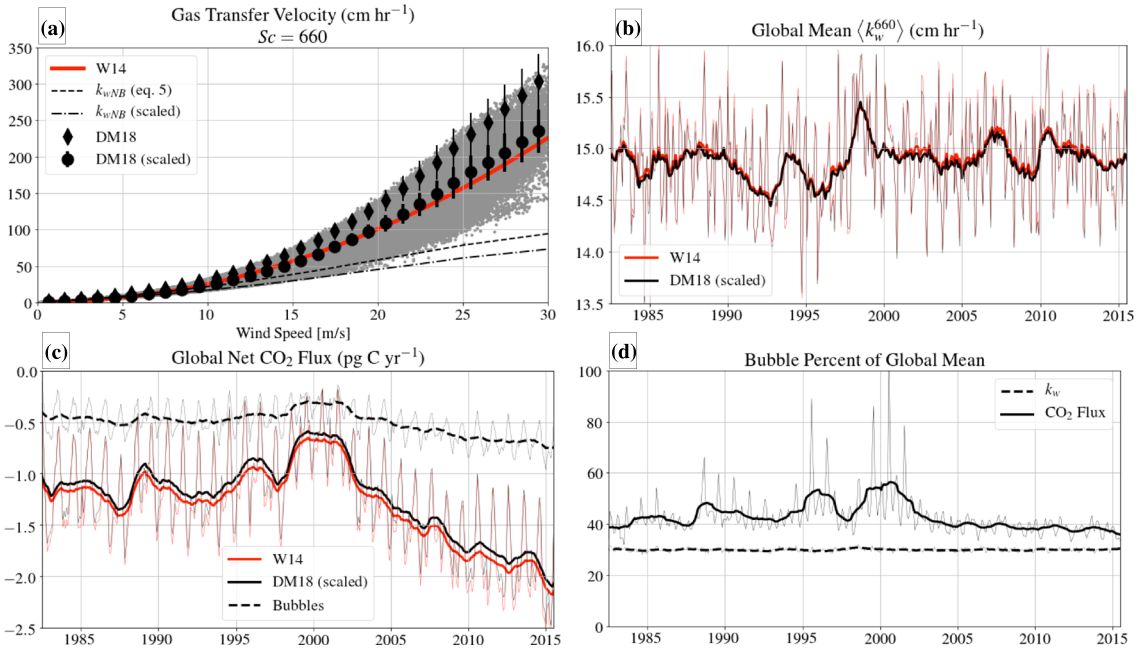

Figure 2. (a) Mean and standard deviation of the gas transfer velocity k_w^{660} in 1 m s^{-1} wind speed bins. Sea-state dependent (DM18) k_w^{660} values are computed from wind speed and significant wave height and shown for (diamonds) original coefficients (equation (3) using equations (4) and (5)) with dashed line for non-bubble component and (squares) reduced coefficients (equation (3) applying 77.5% to equations (4) and (5)) with dot-dashed line for non-bubble component. The wind-only parameterization (W14) for k_w^{660} (equation (2)) is shown in thick red line. One year of data spread is plotted for the scaled DM18 method in gray dots. (b) Time variation of global mean k_w^{660} from the scaled sea-state DM18 (black) and wind-only W14 (red) formulations. (c) Time variation of net global CO_2 flux from the scaled sea-state DM18 (net flux as solid black, with bubble supported flux as dashed line) and wind-only W14 (net flux as red line) formulations. (d) Time variation of gas transfer bubble percentage k_{wB}^{660}/k_w^{660} (dashed) and net CO_2 flux bubble percentage (solid). In panels (b), (c), and (d) the thin lines are instantaneous values while thick lines are 12-month running mean.

5.1. Seasonal Climatology

At a given time, spatial patterns of large transfer velocities are complex and follow mesoscale atmospheric storm events (10–100 km) characterized by strong winds and waves. The differences of the gas transfer velocity from the sea-state dependent formulation (DM18) and the wind-only formulation (W14) are shown for the climatoligical January and July mean ($k_w^{DM18} - k_w^{W14}$, Figures 3a and 3d). The patterns in the difference between the two formulations show some prevailing differences due to basin-scale variability in sea-state, such as enhanced values in the eastern North Atlantic. However, the climatological differences also reflect any differences in the shape of the mean gas transfer velocity as a function of wind speed.

The shape difference is explained because the wind-only gas transfer velocity is strictly a quadratic function of wind speed. For the sea-state dependent formulation, the non-bubble gas transfer dominates at low wind and is linear with wind speed, but the bubble gas transfer goes as $u_*^{5/3} Hs^{2/3}$ and dominates at high winds. Thus, even though the global mean in k_w is similar between the two formulations, the mean value of each at a given wind speed is different and dominates the signal seen in Figures 3a and 3d. To isolate the sea-state effect from the above bias, we introduce $\widetilde{k_w^{DM18}}$ as the average value of the gas transfer velocity at a given wind speed (e.g., the black circles in Figure 2a) and solve for the sea-state induced difference as $\Delta^w k_w = k_w^{DM18} - \widetilde{k_w^{DM18}}$. The January and July climatological mean sea-state differences, $\Delta^w k_w$, are shown in Figures 3b and 3e. The patterns show basin-scale patterns of enhanced and suppressed gas transfer velocity that are solely due to prevailing wind and sea-state patterns. The large regions shaded in red (e.g., North Atlantic and North Pacific in January and Southern Ocean year-round) highlight regions where bubble contributions lead to enhanced gas transfer. This sea-state dependent effect reaches up to 10% of the local gas transfer velocity.

The root-mean-square difference between the sea-state dependent formulation (k_w^{DM18}) and the wind mean ($\widetilde{k_w^{DM18}}$) indicates the degree of added variability due to the sea-state and is given by $\sqrt{\sum (\Delta^w k_w)^2} = \sqrt{\sum \left(k_w^{DM18} - \widetilde{k_w^{DM18}} \right)^2}$ (Figures 3c and 3f). The global patterns for $\sqrt{\sum (\Delta^w k_w)^2}$ are similar to those for $\Delta^w k_w$, but with values up to three times higher (Figures 3b and 3e). This indicates that induced accumulated

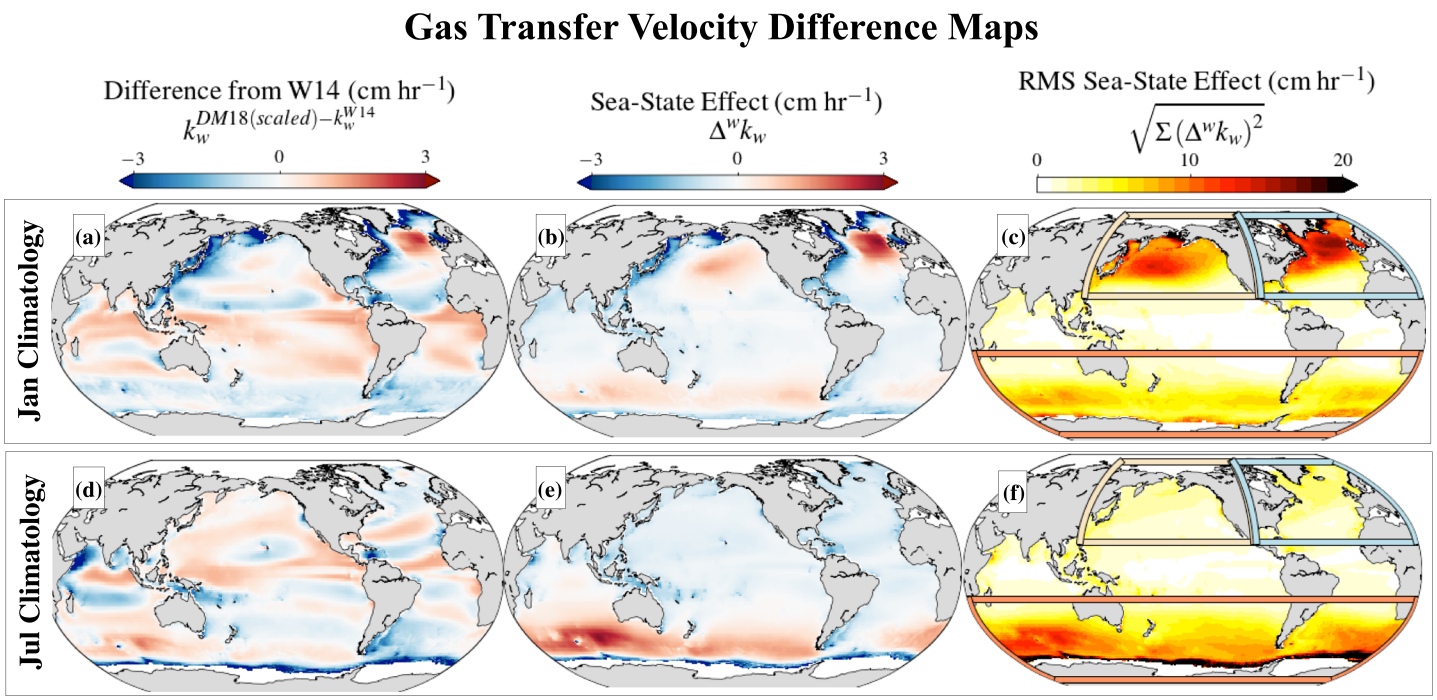

Figure 3. January and July climatological mean from 1982 to 2015 of (a, d) k_w^{DM18} - k_w^{W14}; (b, e) sea-state dependence $\Delta^w k_w = k_w^{DM18} - \widetilde{k_w^{DM18}}$ defined as the full gas transfer velocity calculation minus the wind speed dependent mean $\widetilde{k_w^{DM18}}$; and (c, f) sea-state induced variability $\sqrt{\sum(\Delta^w k_w)^2} = \sqrt{\sum\left(k_w^{DM18} - \widetilde{k_w^{DM18}}\right)^2}$. Note that these figures all use the 77.5% scaling factor in the DM18 approach. Colored boxes in panels (c) and (f) denote the regions for averaging (North Pacific, North Atlantic, and Southern Ocean) in Figure 4.

gas transfer variability due to differences in sea-state is up to 30% in regions of high wave activity in higher latitudes.

5.2. Regional Climatology

We further characterize the role of the sea-state in the transfer velocity by diagnosing their seasonality globally and in three regions of high wind-wave activity. The three regions are the North Atlantic (20–80°N), North Pacific (20–80°N), and Southern Ocean (20–80°S), which are marked in Figures 3c and 3f. The monthly averaged gas transfer velocities for the sea-state dependent method (DM18 w/ 77.5% scale factor) and the corresponding net CO_2 flux are given in Figures 4a and 4b. These quantities show significant seasonal variability that differs in magnitude and phase depending on the region. The gas transfer velocities and net fluxes are enhanced in the winter regions due to higher mean winds and increased frequencies of storms. We next investigate the sea-state induced variability to both the gas transfer velocity (defined as spatial averages of $\sqrt{\sum(\Delta^w k_w)^2}$ in Figure 4c) and net CO_2 flux (defined as spatial averages of $\sqrt{\sum(\Delta^w F_{CO_2})^2}$ in Figure 4d). The added variability also follows a seasonal cycle in these regions, showing that sea-state induced variability increases in winter due to storm activity.

We observe that the sea-state driven variability of the gas transfer velocity is about 8% globally with small seasonal variation (Figure 4e). Similar numbers are found for the Southern Ocean, with only a small seasonal cycle. However, both the North Pacific and North Atlantic exhibit enhanced variability of the gas transfer velocity to about 10% in winter time, with reduced variability of about 5% in summer. This seasonality in the northern basins again suggests that winter storms play an important role for bubble-driven gas transfer velocity.

We compute similar metrics of seasonality both globally and regionally for the CO_2 flux. We find striking differences in CO_2 flux from gas transfer velocity due to the weighting by the different CO_2 uptake and emission patterns dictated by the sign of the partial pressure $\Delta\, p_{CO_2}$. We also note significantly more interannual variability for CO_2 flux than gas transfer velocity (see Figure 4b), which can result in different variability of

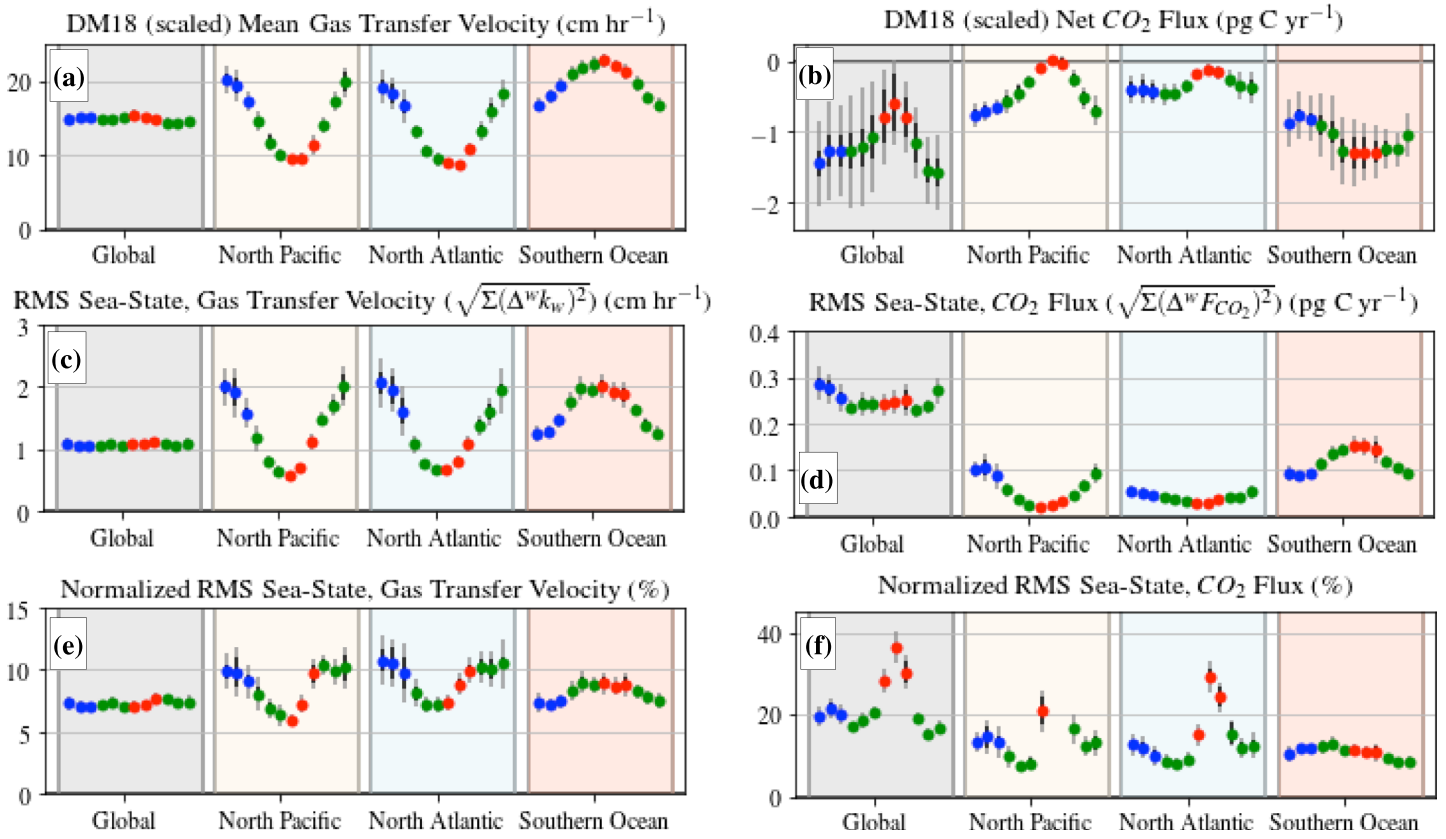

Figure 4. Monthly median values and percentiles for global and key regions of gas transfer velocity, flux, and sea-state added variability. (a) Mean gas transfer velocity, (b) net CO_2 flux computed for the scaled sea-state dependent method $F_{CO_2} = k_w^{DM18} \Delta p_{CO_2}$, (c) root-mean-square difference of sea-state effect, for gas transfer velocity $\sqrt{\sum (\Delta^w k_w)^2} = \sqrt{\sum \left(k_w^{DM18} - \widetilde{k_w^{DM18}} \right)^2}$, and (d) net CO_2 flux $\sqrt{\sum (\Delta^w F_{CO_2})^2} = \sqrt{\sum \left(F_{CO_2}^{DM18} - \widetilde{F_{CO_2}^{DM18}} \right)^2}$. Panels (e) and (f) show the root-mean-square difference expressed as percentage (middle panels divided by top panels) for (e) gas transfer velocity and (f) net CO_2 flux (net CO_2 flux percentages are masked when the mean is less than 0.01 pg C year^{-1}). Markers are colored as blue for northern hemisphere winter (JFM), red for southern hemisphere winter (JAS), and green for other months. The dark black error bars show the 25th–75th percentile range, and the light gray error bars indicate the 5th–95th percentile range.

the sea-state effect (panel d) compared to the gas transfer velocity (panel c). The added variability by considering sea-state when computing CO_2 fluxes is increased to about 10% in the Southern Ocean and to between 10% and 20% in the winter seasons in the North Atlantic and North Pacific. In the summer months, higher fractional variability is observed in the North Atlantic (Figure 4f) that relates to the small regionally averaged flux (Figure 4b). To avoid overstating these fractional variabilities we mask out months where the net flux is approximately zero (August and September). Note that these estimates are limited to an extent because the data set only has monthly means of $\Delta\, p_{CO_2}$, and because the gas transfer velocity and the partial pressure are computed independently from one another while in reality they form a coupled system.

6. Discussion and Conclusion

In this study we apply globally the sea-state dependent parameterization of the gas transfer velocity proposed by Deike and Melville (2018) and investigate how it differs from a traditional wind-only parameterization. The global mean gas transfer velocity from the sea-state dependent formulation is constructed to be similar to the global mean gas transfer velocity of the wind-only formulation that is commonly used when computing global gas exchange budgets. This allows us to quantify the induced variability of the sea-state formulation relative to a wind-only formulation and to estimate the bubble fraction of the gas transfer.

We demonstrate that bubbles contribute about 30% of the gas transfer velocity globally and between 35% and 50% of the globally integrated flux of carbon dioxide, with significant interannual variability due to the variability of the carbon dioxide partial pressure difference. We find that bubbles contribute more than 40%

of the net seasonally averaged gas transfer velocity in the Southern Ocean and North Atlantic and Pacific, thereby playing a significant role in air-sea flux of gases such as carbon dioxide in certain regions over seasonal time frames. Spatially there are many tropical regions where the bubble contribution can be significantly less than this (or nearly absent), confirming significant variability to the mechanisms driving air-sea gas flux. The bubble contribution to net CO_2 flux suggests that improved k_w parameterizations with variability due to surface waves, for CO_2 but also other gases, may improve coupled model fidelity. We find two primary effects of sea-state dependent parameterization of air-sea carbon dioxide fluxes:

1. Large root-mean-square sea-state variability in both air-sea CO_2 flux and gas transfer velocity that reflect daily and small scale (50–100 km) variability associated with strong winds and transient wave evolution during atmospheric storms (Figures 3c and 3f). This effect indicates that sea-state differences contribute variability up to 30% locally and 10% over large regions in high-latitude winters for high-frequency (weather scale) events that have potential to impact regional fluxes.
2. Coherent basin-scale spatial patterns of sea-state dependence (Figures 3b and 3e) that primarily reflect differences associated with large-scale wind and wave patterns. This indicates that sea-state effects favor gas transfer in regions where waves are more developed due to wind direction and persistence, such as eastern regions of the North Atlantic and North Pacific and the Southern Ocean.

These two primary results indicate that sea-state dependent gas transfer parameterizations can significantly reduce uncertainties in air-sea gas-flux estimation ranging from time and spatial scales associated with atmospheric weather to global and climate scales.

There are limitations of our approach that must be investigated in future work. First, the resolution of wind and wave data used here does not fully resolve weather scale variability and therefore likely underestimates weather scale induced variability in gas transfer. The implications of high-frequency variability for parameterizing transfer velocity and carbon dioxide flux in coupled models is not yet understood. The accumulated flux variability in this study is likely amplified due to computing the air-sea carbon dioxide flux using global reconstruction of the partial pressure difference $\Delta\, p_{CO_2}$. It therefore remains unclear how the sea-state dependence of the gas transfer velocity will effect coupled simulations. To investigate such implications, studies resolving the necessary high-frequency temporal resolution could be achieved by specifically designed field campaigns and through sensitivity tests in coupled simulations. The effects on ocean interior CO_2 concentrations in models are particularly worth investigating, since regions with high variability of the CO_2 flux due to sea-state in this study include the Southern Ocean and the North Atlantic, both regions of deep-water production and CO_2 export (e.g., Sabine et al., 2004). Importantly the largest bubble impacts occur in winter, when ocean mixed layer depths are deepest, which could lead to enhanced model ocean interior CO_2 uptake through nonlinear rectification effects related to winter mode water ventilation. Finally, we note that for this experiment we used the bulk parameterization from Deike and Melville (2018) that only accounts for the significant wave height and significantly reduces the computational requirement. This approach may underestimate the variability due to sea-state in the fluxes versus using the high-resolution spectral representation of the wave and wave breaking statistics. This parameterization is based on a more complete formulation that accurately represents high-frequency (full spectral) complexity of the wave and wave breaking fields. These points will be investigated in the future using recent progress in modeling the breaking statistics and the wave spectrum (Romero, 2019).

Acknowledgments
We acknowledge support from the Cooperative Institute for Modeling the Earth's System at Princeton University and the Carbon Mitigation Initiative through Princeton's Environmental Institute at Princeton University. We thank Alistair Adcroft, Seth Bushinsky, John Dunne, Stephen Griffies, and Laure Resplandy for helpful discussions related to this work. We acknowledge comments of David Woolf and an anonymous reviewer that improved the manuscript. All data used in preparing this work are publicly available from the addresses and citations provided. The WAVEWATCH-III model is available online (https://github.com/NOAA-EMC/WW3). The significant wave height and u_* fields produced for this study are available online (doi.org/10.5281/zenodo.3626120).

NOAANA14OAR4320106National Oceanic and Atmospheric Administration

References

Adcroft, A., Anderson, W., Balaji, V., Blanton, C., Bushuk, M., Dufour, C. O., et al. (2019). The GFDL global ocean and sea ice model OM4.0: Model description and simulation features. *Journal of Advances in Modeling Earth Systems*, *11*, 3167–3211. https://doi.org/10.1029/2019MS001726

Ardhuin, F., Rogers, W. E., Babanin, A. V., Filipot, J., Magne, R., Roland, A., et al. (2010). Semiempirical dissipation source functions for ocean waves. Part I: Definition, calibration, and validation. *Journal of Physical Oceanography*, *40*, 1917–1941.

Bell, T. G., Landwehr, S., Miller, S. D., Bruyn, W. J. D., Callaghan, A. H., Scanlon, B., et al. (2017). Estimation of bubble-mediated air-sea gas exchange from concurrent DMS and CO_2 transfer velocities at intermediate-high wind speeds. *Atmospheric Chemistry and Physics*, *17*(14), 9019–9033.

Blomquist, B. W., Brumer, S. E., Fairall, C. W., Huebert, B. J., Zappa, C. J., Brooks, I. M., et al. (2017). Wind speed and sea state dependencies of air-sea gas transfer: Results from the high wind speed gas exchange study (hiwinGS). *Journal of Geophysical Research: Oceans*, *122*, 8034–8062. https://doi.org/10.1002/2017JC013181

Brumer, S. E., Zappa, C. J., Blomquist, B. W., Fairall, C. W., Cifuentes-Lorenzen, A., Edson, J. B., et al. (2017). Wave-related Reynolds number parameterizations of CO_2 and DMS transfer velocities. *Geophysical Research Letters*, *44*, 9865–9875. https://doi.org/10.1002/2017GL074979

Chawla, A., Spindler, D. M., & Tolman, H. L. (2013). Validation of a thirty year wave hindcast using the Climate Forecast System Reanalysis winds. *Ocean Modelling*, *70*, 189–206.

Deike, L., Lenain, L., & Melville, W. K. (2017). Air entrainment by breaking waves. *Geophysical Research Letters*, *44*, 3779–3787. https://doi.org/10.1002/2017GL072883

Deike, L., & Melville, W. K. (2018). Gas transfer by breaking waves. *Geophysical Research Letters*, *45*, 10,482–10,492.

Deike, L., Melville, W. K., & Popinet, S. (2016). Air entrainment and bubble statistics in breaking waves. *Journal of Fluid Mechanics*, *801*, 91–129.

Edson, J. B., Jampana, V., Weller, R. A., Bigorre, S. P., Plueddemann, A. J., Fairall, C. W., et al. (2013). On the exchange of momentum over the open ocean. *Journal of Physical Oceanography*, *43*, 1589–1610.

Fairall, C. W., Yang, M., Bariteau, L., Edson, J., Helmig, D., McGillis, W., et al. (2011). Implementation of the coupled ocean-atmosphere response experiment flux algorithm with CO_2, dimethyl sulfide, and O_3. *Journal of Geophysical Research*, *116*, C00F09. https://doi.org/10.1029/2010JC006884

Fangohr, S., & Woolf, D. K. (2007). Application of new parameterizations of gas transfer velocity and their impact on regional and global marine CO_2 budgets. *Journal of Marine Systems*, *66*(4), 195–203. https://doi.org/10.1016/j.jmarsys.2006.01.012

Farmer, D. M., McNeil, C. L., & Johnson, B. D. (1993). Evidence for the importance of bubbles in increasing air-sea gas flux. *Nature*, *361*, 620–623.

Garbe, C. S., Rutgersson, A., Boutin, J., de Leeuw, G., Delille, B., Fairall, C. W., et al. (2014). *Transfer across the air-sea interface* (pp. 55–112). Berlin Heidelberg: Springer.

Griffies, S. M., Danabasoglu, G., Durack, P. J., Adcroft, A. J., Balaji, V., Böning, C. W., et al. (2016). OMIP contribution to CMIP6: Experimental and diagnostic protocol for the physical component of the Ocean Model Intercomparison Project. *Geoscientific Model Development*, *9*(9), 3231–3296.

Ho, D. T., Law, C. S., Smith, M. J., Schlosser, P., Harvey, M., & Hill, P. (2006). Measurements of air-sea gas exchange at high wind speeds in the Southern Ocean: Implications for global parameterizations. *Geophysical Research Letters*, *33*, L16611. https://doi.org/10.1029/2006GL026817

Ho, D. T., Wanninkhof, R., Schlosser, P., Ullman, D. S., Hebert, D., & Sullivan, K. F. (2011). Toward a universal relationship between wind speed and gas exchange: Gas transfer velocities measured with 3He/SF6 during the Southern Ocean Gas Exchange Experiment. *Journal of Geophysical Research*, *116*, C00F04. https://doi.org/10.1029/2010JC006854

IPCC (2014). Climate change 2014: Synthesis report. In Core Writing Team, R. K. Pachauri, & L. A. Meyer (Eds.), *Contribution of working groups I, II and III to the fifth assessment report of the intergovernmental panel on climate change* (pp. 151). Geneva, Switzerland: IPCC.

Keeling, R. F. (1993). On the role of large bubbles in air-sea gas exchange and supersaturation in the ocean. *Journal of Marine Research*, *51*(2), 237–271.

Kobayashi, S., Ota, Y., Harada, Y., Ebita, A., Moriya, M., Onoda, H., et al. (2015). The JRA-55 reanalysis: General specifications and basic characteristics. *Journal of the Meteorological Society of Japan*, *93*(1), 5–48.

Landschützer, P., Gruber, N., Bakker, D. C. E., & Schuster, U. (2014). Recent variability of the global ocean carbon sink, Global Biogeochem. *Cycles*, *28*, 927–949.

Large, W. G., & Yeager, S. (2009). The global climatology of an interannually varying air-sea flux data set. *Climate Dynamics*, *33*, 341–364. https://doi.org/10.1007/s00382-008-0441-3

Le Quére, C. (2018). Carbon budget 2018. *Earth System Science Data*, *10*, 2141–2194.

Leighton, T. G., Coles, D. G. H., Srokosz, M., White, P. R., & Woolf, D. K. (2018). Asymmetric transfer of CO_2, across a broken sea surface. *Nature Scientific Reports*, *8301*(8), 1–9.

Liang, J.-H., Deutsch, C., McWilliams, J. C., Baschek, B., Sullivan, P. P., & Chiba, D. (2013). Parameterizing bubble-mediated air-sea gas exchange and its effect on ocean ventilation. *Global Biogeochemical Cycles*, *27*(3), 894–905.

Liu, Q., Babanin, A., Fan, Y., Zieger, S., Guan, C., & Moon, I.-J. (2017). Numerical simulations of ocean surface waves under hurricane conditions: Assessment of existing model performance. *Ocean Modelling*, *118*, 73–93.

Pfeil, B., Olsen, A., Bakker, D. C. E., Hankin, S., Koyuk, H., Kozyr, A., et al. (2012). A uniform, quality controlled Surface Ocean CO_2 Atlas (SOCAT). *Earth System Science Data Discussions*, *5*(2), 735–780.

Resplandy, L., Keeling, R. F., Rödenbeck, C., Stephens, B. B., Khatiwala, S., Rodgers, K. B., et al. (2018). Revision of global carbon fluxes based on a reassessment of oceanic and riverine carbon transport. *Nature Geoscience*, *11*(7), 504–509.

Rödenbeck, C., Bakker, D. C. E., Gruber, N., Iida, Y., Jacobson, A. R., Jones, S., et al. (2015). Data-based estimates of the ocean carbon sink variability–first results of the Surface Ocean pCO_2 mapping intercomparison (SOCOM). *Biogeosciences*, *12*, 7251–7278.

Romero, L. (2019). Distribution of surface wave breaking fronts. *Geophysical Research Letters*, *46*, 10,463–10,474.

Sabine, C. L., Feely, R. A., Gruber, N., Key, R. M., Lee, K., Bullister, J. L., et al. (2004). The Oceanic Sink for Anthropogenic CO_2. *Science*, 367–371.

Sabine, C. L., Hankin, S., Koyuk, H., Bakker, D. C. E., Pfeil, B., Olsen, A., et al. (2012). Surface Ocean CO_2 Atlas (SOCAT) gridded data products. *Earth System Science Data Discussions*, *5*(2), 781–804.

Smith, M. J., Walker, C. F., Bell, T. G., Harvey, M. J., Saltzman, E. S., & Law, C. S. (2018). Gradient flux measurements of sea–air DMS transfer during the Surface Ocean Aerosol Production (SOAP) experiment. *Atmospheric Chemistry and Physics*, *18*(8), 5861–5877.

Taboada, F. G., Stock, C. A., Griffies, S. M., Dunne, J., John, J. G., Small, R. J., & Tsujino, H. (2019). Surface winds from atmospheric reanalysis lead to contrasting oceanic forcing and coastal upwelling patterns. *Ocean Modeling*, *133*, 79–111.

Takahashi, T., Feely, R. A., Weiss, R. F., Wanninkhof, R. H., Chipman, D. W., Sutherland, S. C., & Takahashi, T. T. (1997). Global air-sea flux of CO_2: An estimate based on measurements of sea-air pCO_2 difference Proc. *Proceedings of the National Academy of Sciences of the United States of America*, *94*, 8292–8299.

The WAVEWATCH III Development Group (WW3DG) (2016). User manual and system documentation of WAVEWATCH III version 5.16, *Tech. Note 329, NOAA/NWS/NCEP/MMAB*, 326. + Appendices.

Thomson, J., Girton, J. B., Jha, R., & Trapani, A. (2018). Measurements of directional wave spectra and wind stress from a wave glider autonomous surface vehicle. *Journal of Atmospheric and Oceanic Technology*, *35*, 347–363. https://doi.org/10.1175/JTECH-D-17-0091.1

Thorpe, S. A., & Humphries, P. N. (1980). Bubbles and breaking waves. *Nature*, *283*, 463–465.

Tsujino, H., Urakawa, S., Nakano, H., Small, R. J., Kim, W. M., Yeager, S. G., et al. (2018). JRA-55 Based surface dataset for driving ocean-sea-ice models (JRA55-do). *Ocean Modelling*, *130*, 79–139.

Wanninkhof, R. (2014). Relationship between wind speed and gas exchange over the ocean revisited. *Limnology and Oceanography Methods*, *12*(6), 351–362.

Wanninkhof, R., Asher, W. E., Ho, D. T., Sweeney, C., & McGillis, W. R. (2009). Advances in quantifying air-sea gas exchange and environmental forcing. *Annual Review of Marine Science*, *1*, 213–44.

Weiss, R. F. (1974). Carbon dioxide in water and seawater: The solubility of a non-ideal gas. *Marine Chemistry*, *2*, 203–215.
Woolf, D. K. (1993). Bubbles and the air-sea transfer velocity of gases. *Atmosphere-Ocean*, *31*(4), 517–540.
Woolf, D. K. (1997). Bubbles and their role in gas exchange, *The Sea Surface and Global Change*. Cambridge, UK: Cambridge University Press.
Woolf, D. K. (2005). Parameterization of gas transfer velocities and sea-state-dependent wave breaking. *Tellus*, *57B*, 87–94.
Woolf, D. K., Shutler, J. D., Goddijn-Murphy, L., Watson, A. J., Chapron, B., Nightingale, P. D., et al. (2019). Key uncertainties in the recent air-sea flux of CO_2. *Global Biogeochemical Cycles*, *33*, 1548–1563. https://doi.org/10.1029/2018GB006041
Yang, M., Blomquist, B., & Nightingale, P. D. (2014). Air-sea exchange of methanol and acetone during hiwinGS: Estimation of air phase, water phase gas transfer velocities. *Journal of Geophysical Research: Oceans*, *119*, 7308–7323. https://doi.org/10.1002/2014JC010227
Zhang, X. (2012). Contribution to the global air sea CO_2 exchange budget from asymmetric bubble-mediated gas transfer. *Tellus B*, *64*(1), 17,260.
Zhao, D., Toba, Y., Suzuki, Y., & Komori, S. (2003). Effect of wind waves on air-sea gas exchange: Proposal of an overall CO_2 transfer velocity formula as a function of breaking-wave parameter. *Tellus B*, *55*(2), 478–487.
Zweng, M. M, Reagan, J. R., Antonov, J. I., Locarnini, R. A., Mishonov, A. V., Boyer, T. P., et al. (2013). World Ocean Atlas 2013. Volume 2: Salinity NOAA Atlas NESDIS (74).